Bulklike Vibrational Coupling of Surface Water Revealed by Sum-Frequency Generation Spectroscopy

Kuo-Yang Chiang,[1,*] Xiaoqing Yu,[1,*] Chun-Chieh Yu,[1] Takakazu Seki,[1] Shumei Sun,[2] Mischa Bonn,[1,†] and Yuki Nagata[1,‡]

[1]*Max Planck Institute for Polymer Research, Ackermannweg 10, 55128 Mainz, Germany*

[2]*Department of Physics and Applied Optics Beijing Area Major Laboratory, Beijing Normal University, Beijing 100875, China*

(Received 3 December 2022; revised 10 October 2023; accepted 30 October 2023; published 20 December 2023)

Vibrational coupling between interfacial water molecules is important for energy dissipation after on-water chemistry, yet intensely debated. Here, we quantify the interfacial vibrational coupling strength through the linewidth of surface-specific vibrational spectra of the water's O—H (O—D) stretch region for neat H_2O/D_2O and their isotopic mixtures. The local-field-effect-corrected experimental SFG spectra reveal that the vibrational coupling between hydrogen-bonded interfacial water O—H groups is comparable to that in bulk water, despite the effective density reduction at the interface.

DOI: 10.1103/PhysRevLett.131.256202

Water surfaces are omnipresent and essential for various interfacial phenomena such as evaporation [1–3] and on-water surface chemical reactions [4,5]. The characteristic hydrogen-bond (H-bond) structure at the interface gives rise to several peculiar properties of liquid water surfaces. The interface constitutes a confined environment for molecules to generate incomplete solvation, accelerating specific chemical reactions compared to the bulk [4,5]. Such (photo-)chemical reactions on the water surface release excess energy at the surface, which is generally dissipated efficiently into the bulk. Inversely, the process of evaporation requires the instantaneous pooling of excess energy to enable the release of individual water molecules into the vapor phase [1]. One of the energy transfer pathways involves an efficient exchange of vibrational energy quanta between O—H groups—both within one water molecule (intramolecular) and between water molecules [intermolecular, see Figs. 1(a) and 1(b)]. Couplings between the transition dipole moments enable such an energy transfer [6,7]. In pure H_2O, energy transfer between the O—H stretch vibrations is highly effective, taking place on <200 fs timescales [6–9].

This strong vibrational coupling is also reflected in the linear, infrared absorption spectrum of bulk liquid water [10,11]: the coupling between different O—H groups is sufficiently strong that it leads to a substantial broadening of the O—H stretch response. Indeed, this broadening disappears when the coupling between the O—H stretch vibrations is switched off by isotopically diluting O—H groups in D_2O (i.e., when investigating the O—H stretch vibration of HOD in D_2O) [10]. In particular, the appearance of a 3000–3300 cm^{-1} shoulder has been assigned to a vibrational quantum being delocalized over ∼10 water molecules through intermolecular vibrational coupling [11,12]. In contrast, intramolecular vibrational coupling is known to play a minor role in the lineshape and width of the O—H stretch band of bulk water [10,11,13].

While the effect of coupling on the vibrational spectral response in bulk is uncontested, this is not true for the surface, and different conclusions have been drawn on the extent of vibrational coupling between interfacial water molecules. As a second-order nonlinear optical ($\chi^{(2)}$) technique, heterodyne-detected sum-frequency generation (HD-SFG) spectroscopy has been used to selectively probe the response of the few topmost water layers at the air-water interface [14–17]. The SFG spectrum of water's O—H stretch mode shows a positive 3700 cm^{-1} and a negative 3400 cm^{-1} feature [18,19]. The 3700 cm^{-1} peak arises from the free O—H stretch mode of the topmost water molecules with one H-bond donor. These free O—H groups are largely uncoupled from the bulk and require structural rearrangement to transfer vibrational energy to the bulk, by H bonding with subsurface water molecules [17,20]. The 3400 cm^{-1} peak is attributed to the H-bonded O—H group of interfacial water molecules [19]. It has been debated to what extent the negative band arises not only from the intrinsic vibrational feature of H-bonded O—H groups but also from the intra- and intermolecular vibrational coupling of the O—H stretch mode [15,16,21–23].

Attempts to quantify the vibrational couplings of interfacial water molecules have been made using isotopic

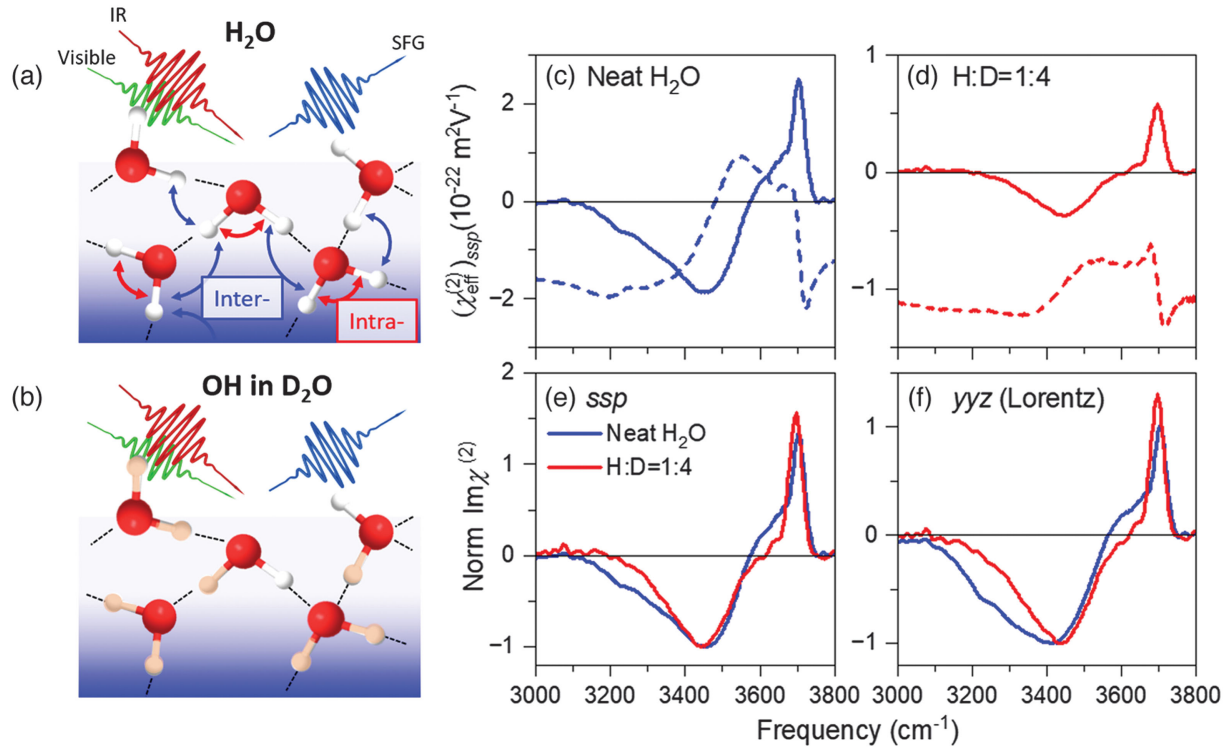

FIG. 1. (a),(b) The schematic of intramolecular and intermolecular vibrational couplings in the (a) neat H_2O and (b) isotopically diluted water solution. The intramolecular and intermolecular vibrational couplings represent the coupling between the transition dipole moments of each O—H group. (c),(d) Experimentally measured $(\chi^{(2)}_{\text{eff}})_{ssp}$ spectra of vibrational O—H stretch mode at (c) the air-neat H_2O interface and (d) the air/H:D = 1:4 isotopically diluted water interface. Solid and dashed lines represent the imaginary and real parts of spectra, respectively. (e) $\text{Im}(\chi^{(2)}_{\text{eff}})_{ssp}$ and (f) $\text{Im}\chi^{(2)}_{yyz}$ spectra. All spectra were normalized to the negative peak maxima.

dilution of water in (time-resolved) SFG measurements [14–16,20,22–27] and SFG spectra simulations [14,21,22,28,29]. The resulting conclusions on the vibrational coupling of water at the air-water interface differ substantially between the different studies. For example, previous simulations show a drastic change in the negative band in the $\text{Im}\chi^{(2)}_{yyz}$ spectra upon isotopic dilution [21,28], where the *xy* and *xz* planes form the surface and the incident plane of the beams, respectively. In contrast, experiments [22,26] have indicated that the change of the $\text{Im}\chi^{(2)}_{yyz}$ spectra upon the isotope dilution is substantially less pronounced than that of the infrared (IR) and Raman spectra of bulk water. As such, the impact of the vibrational coupling on the SFG spectra of the O—H stretch mode of water, and thereby the efficacy of vibrational energy transfer at the surface, is still underdebated.

To address this question, we perform HD-SFG measurements using the *ssp* polarization combination at the air (neat) water and air (isotopically) diluted water interfaces in the O—H stretch and O—D stretch regions, where, *ssp* denotes the *s*-, *s*-, and *p*-polarized SFG, visible, and IR beams. While the measured raw $[\text{Im}(\chi^{(2)}_{\text{eff}})_{ssp}]$ spectra for neat and isotopically diluted water are fairly similar, the molecular responses embodied by the $\text{Im}\chi^{(2)}_{yyz}$ spectra are very different. The $\text{Im}\chi^{(2)}_{yyz}$ spectra are obtained from the $(\chi^{(2)}_{\text{eff}})_{ssp}$ spectra by correcting for local field effects on the Fresnel factors [19]. The experimentally deduced O—H stretch $\text{Im}\chi^{(2)}_{yyz}$ spectra at the air/HOD in D_2O interface agree with the simulated data, ensuring the robustness of the current analysis. Our results resolve the controversy on the strength of vibrational coupling of surface water [14–16,21,22,26,28].

First, we measured the HD-SFG spectra of the vibrational O—H stretch mode from the interfaces of air-neat H_2O and air/H_2O—D_2O mixture with an H:D ratio of 1:4. The measured $(\chi^{(2)}_{\text{eff}})_{ssp}$ spectra are displayed in Figs. 1(c) and 1(d) for the neat H_2O and H:D = 1:4 water samples, respectively. The $\text{Im}(\chi^{(2)}_{\text{eff}})_{ssp}$ amplitude of the neat H_2O sample is ~5 times larger than that of the H:D = 1:4 isotopically diluted water sample. Figure 1(e) compares the $\text{Im}\,(\chi^{(2)}_{\text{eff}})_{ssp}$ spectra of neat and isotopically diluted water. A cursory inspection of the data indicates rather limited vibrational coupling at the interface, given the similarity between the two spectra. A more detailed comparison indicates five main changes in the spectral features. (i) The free O—H peak is redshifted by 8 cm^{-1} upon isotopic dilution, consistent with Refs. [24,26]. This redshift is due

to the missing energy splitting of the free O—H group and H-bonded O—H group in the same water molecule [24]. (ii) The 3600 cm^{-1} shoulder peak vanishes upon isotopic dilution, because the antisymmetric stretch peak of H-bonded H_2O molecules is absent in the HOD molecule [15,21,24]. (iii) The negative band below 3350 cm^{-1} is slightly reduced in amplitude upon isotopic dilution. (iv) A slight but non-negligible positive band in the 3000–3200 cm^{-1} region is observed for the isotopically diluted H_2O sample, but it is absent in the neat H_2O sample. (v) A 3250 cm^{-1} shoulder is observed for neat H_2O, but is absent for isotopically diluted H_2O, which is attributed to the Fermi resonance present only for pure H_2O [23,30].

To retrieve the true water response $\chi^{(2)}_{yyz}$ from the measured $(\chi^{(2)}_{\rm eff})_{ssp}$ spectra, we have to correct for the local field effects using the Fresnel factors $L_{aa}(\omega_i)$:

$$\chi^{(2)}_{yyz} = (\chi^{(2)}_{\rm eff})_{ssp}/\left(L_{yy}(\omega)L_{yy}(\omega_1)L_{zz}(\omega_2)\sin\beta_2\right), \quad (1)$$

where ω, ω_1, and ω_2 denote the frequencies of the SFG, visible, and IR beams, respectively [19]. $L_{aa}(\omega_i)$ is the aa component of the Fresnel factor at frequency ω_i, and β_2 denotes the incident angle of the IR beam in respect to surface normal. $L_{zz}(\omega_2)$ contains the frequency-dependent interfacial dielectric profile term $[\varepsilon'(\omega)]$ [31], approximated here using the Lorentz model. We demonstrated that the Lorentz model ($\varepsilon' = \varepsilon$, i.e., approximating the interfacial dielectric function by that of bulk water ε) provides an excellent approximation of the interfacial dielectric function for O—H stretch $(\chi^{(2)}_{\rm eff})_{ssp}$ spectra of water [30,32] (See Supplemental Material III [33] for dielectric spectra for H:D = 1:4 isotopically diluted water, which includes Refs. [31,34–37]). The obtained Im $\chi^{(2)}_{yyz}$ spectra are displayed in Fig. 1(f). The trends of (i), (ii), (v) are unchanged in the Im $\chi^{(2)}_{yyz}$ spectra, while trend (iii) is amplified and trend (iv) no longer exists: after removal of Fresnel factor, the vibrational coupling feature in 3100–3400 cm^{-1} is enhanced, and the 3000–3200 cm^{-1} positive band vanishes.

The very broad negative feature for pure H_2O is consistent with the previous simulations [21,28], but at odds with several experimental reports [22,26]. This discrepancy can be traced to the interfacial dielectric profile used in the Fresnel factor correction. Unlike our previous studies using the Lorentz model ($\varepsilon' = \varepsilon$) [30,32], Refs. [22,26] used the slab model $[\varepsilon' = [\varepsilon(\varepsilon+5)/(4\varepsilon+2)]]$, which provides similar line shapes of $\mathrm{Im}\chi^{(2)}_{yyz}$ and $\mathrm{Im}(\chi^{(2)}_{\rm eff})_{ssp}$ spectra [38]; because the $\mathrm{Im}(\chi^{(2)}_{\rm eff})_{ssp}$ spectra of the neat and isotopically diluted H_2O are similar, the processed $\mathrm{Im}\chi^{(2)}_{yyz}$ spectra are similar with the slab model, leading to the conclusion that the impact of the vibrational coupling is weak compared with bulk water [22,26]. Trend (iv) on the top of the constant phase shift of the spectra [38,39] has been debated [16,40], and is attributed to icelike water [15] as well as to nuclear quantum effects [41]. However, our data clearly show that 3000–3200 cm^{-1} positive band feature observed in the $\mathrm{Im}(\chi^{(2)}_{\rm eff})_{ssp}$ spectra (see detailed discussion in the Supplemental Material [33]) vanishes in the $\mathrm{Im}\chi^{(2)}_{yyz}$ spectra; the positive feature results from the Fresnel factor, not from properties of interfacial water [42,43].

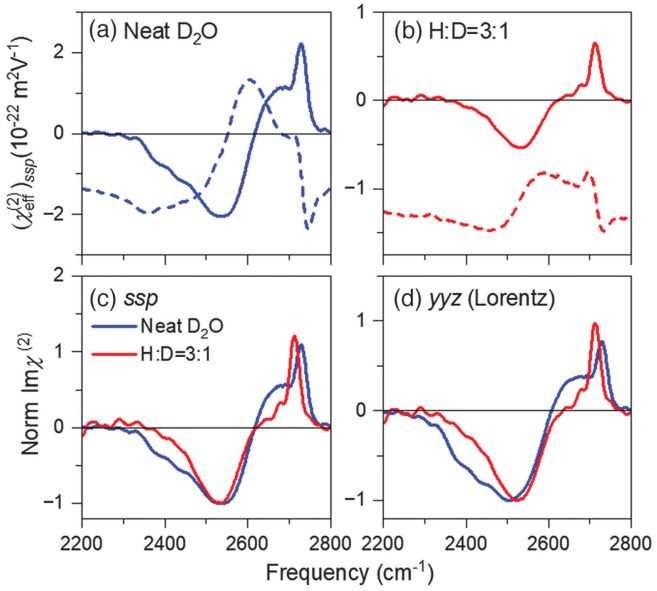

FIG. 2. (a),(b) Experimentally measured $(\chi^{(2)}_{\rm eff})_{ssp}$ spectra of the O—D stretch mode at (a) the air-neat D_2O interface and (b) the air/H:D = 3:1 isotopically diluted water interface. Solid and dashed lines represent the imaginary and real parts of the spectra, respectively. (c),(d) Comparison of (c) $\mathrm{Im}(\chi^{(2)}_{\rm eff})_{ssp}$ and (d) $\mathrm{Im}\chi^{(2)}_{yyz}$ spectra. All spectra were normalized to the negative peak maxima.

Now we turn our focus to SFG spectra of the vibrational O—D stretch mode for the neat D_2O and H_2O—D_2O mixture solution with H:D ratio of 3:1. The measured $(\chi^{(2)}_{\rm eff})_{ssp}$ spectra are displayed in Figs. 2(a) and 2(b), while Figs. 2(c) and 2(d) display the comparison of the $(\chi^{(2)}_{\rm eff})_{ssp}$ and $\mathrm{Im}\chi^{(2)}_{yyz}$ spectra of the neat and isotopically diluted D_2O samples. Trends (ii)–(v) are similarly observed in the O—D stretch region, while the free O—D peak is redshifted by 16 cm^{-1} upon isotopic dilution [24,44]. Similar to the O—H stretch mode, the Fresnel factor correction leaves trends (i), (ii), and (v) unaffected, while trends (iii) and (iv) change through the Fresnel factor correction; the difference of the negative 2450 cm^{-1} band between the neat and isotopically diluted D_2O is enhanced, and the weak positive band in the 2250–2350 cm^{-1} region vanishes after removal of Fresnel factor.

A question arising here is how the Fresnel factor correction affects the spectral shape of the $\mathrm{Im}\chi^{(2)}_{yyz}$ spectra.

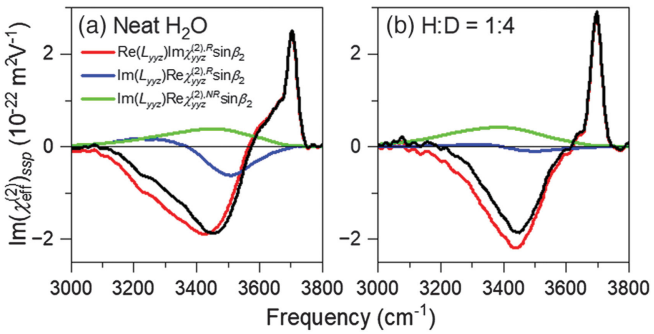

FIG. 3. (a),(b) Decomposition of the $\mathrm{Im}(\chi^{(2)}_{\mathrm{eff}})_{ssp}$ spectra of (a) the air-neat H_2O interface and (b) the air/$H:D = 1:4$ isotopically diluted water interface based on Eq. (2). The black lines represent the measured $\mathrm{Im}(\chi^{(2)}_{\mathrm{eff}})_{ssp}$ spectra. The spectra in panel b were rescaled by a factor of 5. The detailed spectra of L_{yyz} are shown in the Supplemental Material [33].

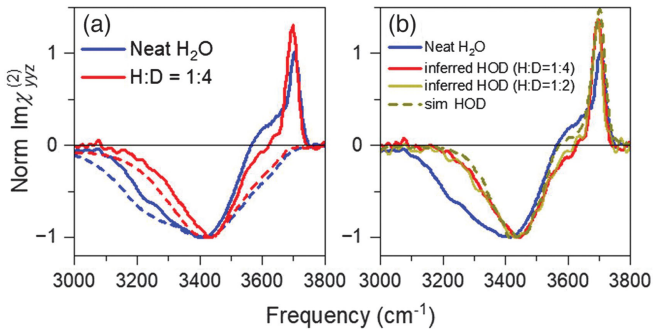

FIG. 4. (a) The comparison of normalized $\mathrm{Im}\chi^{(2)}_{yyz}$ spectra (solid lines) at the interface of the air-neat H_2O and air/$H:D = 1:4$ isotopically diluted water and corresponding bulk $\sqrt{\alpha_{\mathrm{IR}} I_{\mathrm{Raman}}}$ spectra (dashed lines). (b) The inferred $\mathrm{Im}\chi^{(2)}_{yyz,\mathrm{HOD}}$ spectra obtained from the $H:D = 1:2$ and $1:4$ solutions. We also plot the simulated $\mathrm{Im}\chi^{(2)}_{yyz}$ spectrum at air-water interface for HOD in D_2O (see Supplemental Material [33]). All spectra were normalized to the negative peak maxima.

To address this question, we decomposed the $\mathrm{Im}(\chi^{(2)}_{\mathrm{eff}})_{ssp}$ spectra into the three terms;

$$\mathrm{Im}(\chi^{(2)}_{\mathrm{eff}})_{ssp} = \sin\beta_2 \left(\mathrm{Im}L_{yyz}\mathrm{Re}\chi^{(2),NR}_{yyz} + \mathrm{Im}L_{yyz}\mathrm{Re}\chi^{(2),R}_{yyz} + \mathrm{Re}L_{yyz}\mathrm{Im}\chi^{(2),R}_{yyz}\right), \quad (2)$$

where $L_{yy}(\omega)L_{yy}(\omega_1)L_{zz}(\omega_2)$ is abbreviated as L_{yyz} and $\chi^{(2),NR}_{yyz}$ ($\chi^{(2),R}_{yyz}$) denotes the nonresonant (resonant) part of $\chi^{(2)}_{yyz}$. Because $\chi^{(2),NR}_{yyz}$ is real at the neutral interface [45,46], we set $\chi^{(2),NR}_{yyz} = -4 \times 10^{-22}$ m^2 V^{-1}.

The contributions from the individual terms in Eq. (2) are displayed in Figs. 3(a) and 3(b) for neat and isotopically diluted H_2O, respectively. The third term of $\mathrm{Re}L_{yyz}\mathrm{Im}\chi^{(2),R}_{yyz}\sin\beta_2$ resembles the $\mathrm{Im}\chi^{(2),R}_{yyz}$ line shapes for both neat and isotopically diluted H_2O. The first term in Eq. (2), $\mathrm{Im}L_{yyz}\mathrm{Re}\chi^{(2),NR}_{yyz}\sin\beta_2$, lifts up the spectra, generating the positive 3000–3200 cm^{-1} feature in the isotopically diluted H_2O data (trend (iv)). The second term, $\mathrm{Im}L_{yyz}\mathrm{Re}\chi^{(2),R}_{yyz}\sin\beta_2$, shows a positive-negative feature for the neat H_2O, which reduces the negative 3100–3400 cm^{-1} contribution in the $\mathrm{Im}(\chi^{(2),R}_{\mathrm{eff}})_{ssp}$ spectra for neat H_2O (trend (iii)). In contrast, it is negligible for isotopically diluted H_2O, because the non-resonant contribution is not present in this term and thus the amplitude of this term differs ~25 times between the neat H_2O and $H:D = 1:4$ solution, unlike the other terms, which differ ~5 times.

After obtaining the $\mathrm{Im}\chi^{(2)}_{yyz}$ spectra, we discuss the vibrational coupling between the interfacial and bulk water responses by comparing the $\mathrm{Im}\chi^{(2)}_{yyz}$ spectra with the $\sqrt{\alpha_{\mathrm{IR}} I_{\mathrm{Raman}}}$ spectra, where α_{IR} and I_{Raman} are the bulk infrared and Raman signals, respectively [21,26] (See Supplemental Material I.C. and I.D [33] for Raman and IR experiments, which include Refs. [47,48]). We used the $\sqrt{\alpha_{\mathrm{IR}} I_{\mathrm{Raman}}}$ spectra, because SFG is composed of the IR transition and Raman transition [21,26]. Recent studies of the silica-water interfaces have shown the close resemblance between the $\sqrt{\alpha_{\mathrm{IR}} I_{\mathrm{Raman}}}$ feature and the bulklike $\mathrm{Im}\chi^{(3)}$ feature, which results from the diffuse layer in the electric double layer model [49,50], ensuring that the $\sqrt{\alpha_{\mathrm{IR}} I_{\mathrm{Raman}}}$ spectra are the good reference for the bulk signal (see Supplemental Material VIII [33] for the comparison between bulk $\sqrt{\alpha_{\mathrm{IR}} I_{\mathrm{Raman}}}$ spectrum and $\chi^{(3)}$ spectrum, which includes Refs. [51,52]). The data are shown in Fig. 4(a). The full width at half maximum (FWHM) of the negative $\mathrm{Im}\chi^{(2)}_{yyz}$ band reduces by ~31% upon isotopic dilution (from 290 cm^{-1} of neat H_2O to 200 cm^{-1} of $H:D = 1:4$ samples), and the bulk $\sqrt{\alpha_{\mathrm{IR}} I_{\mathrm{Raman}}}$ spectra reduces by ~32% (from 410 to 280 cm^{-1}), indicating a comparable inter- or intramolecular coupling effect between the bulk water and the interfacial water. However, the peak itself is substantially narrower in the interfacial $\mathrm{Im}\chi^{(2)}_{yyz}$ spectra than the bulk $\sqrt{\alpha_{\mathrm{IR}} I_{\mathrm{Raman}}}$ spectra. The reduced amplitude in the <3300 cm^{-1} region in the $\mathrm{Im}\chi^{(2)}_{yyz}$ spectra compared with the bulk can be attributed to the fact that strongly H-bonded O—H groups tend to orient along the surface [53,54], which are SFG-invisible. Furthermore, we computed the negative peak area in the $\mathrm{Im}\chi^{(2)}_{yyz}$ spectra and compared them with the peak area in the $\sqrt{\alpha_{\mathrm{IR}} I_{\mathrm{Raman}}}$ spectra. The reduction of the peak area in the $\mathrm{Im}\chi^{(2)}_{yyz}$ spectra upon isotopically diluting the water is 25%, in good agreement with 24% reduction in the bulk $\sqrt{\alpha_{\mathrm{IR}} I_{\mathrm{Raman}}}$ spectra.

Above, we discussed the spectral shape and coupling effect based on the $\mathrm{Im}\chi^{(2)}_{yyz}$ spectra of neat and isotopically diluted water. However, even the $\mathrm{Im}(\chi^{(2)}_{yyz})$ spectrum of the $H:D = 1:4$ isotopically diluted water contains a small but

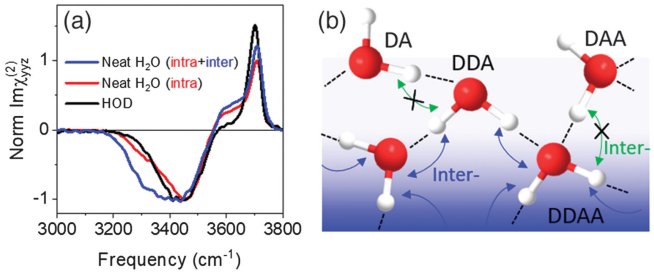

FIG. 5. (a) The simulated $\mathrm{Im}\chi^{(2)}_{yyz}$ spectrum of neat H_2O without intermolecular vibrational coupling (red), together with $\mathrm{Im}\chi^{(2)}_{yyz,\mathrm{HOD}}$ spectrum (black) and neat H_2O $\mathrm{Im}\chi^{(2)}_{yyz}$ spectrum (blue). (b) The schematic of the bulklike intermolecular vibrational couplings of interfacial water. This further illustrates that a small portion of the other O—H group of the interfacial water molecule with the free O—H group (DA and DAA water molecules) does not exhibit bulklike coupling.

non-negligible impact of the vibrational coupling. While we cannot remove the intermolecular coupling entirely, we can remove the contribution from the remnant intramolecular coupling (see Supplemental Material [33]) [15]. Figure 4(b) displays the inferred air/HOD in D_2O $\mathrm{Im}\chi^{(2)}_{yyz}$ spectra together with the corresponding spectrum simulated with the POLI2VS model of water [21,55]. The agreement of the experimentally inferred $\mathrm{Im}\chi^{(2)}_{yyz,\mathrm{HOD}}$ spectra from $\mathrm{H:D} = 1:2$ and $1:4$ solutions (see Supplemental Material [33]) ensures that the $\mathrm{Im}\chi^{(2)}_{yyz,\mathrm{HOD}}$ spectrum is well converged to the infinite diluted HOD in D_2O case. Except for the 3600 cm^{-1} shoulder peak region, the simulated and experimental data agree. This 3600 cm^{-1} signature is overestimated in the simulation due to the missing nuclear quantum effects [30,42]. The overall agreement of the spectral feature demonstrates the robustness of the simulation data and ensures the validity of the analysis performed here.

We confirmed that the surface and bulk have comparably strong vibrational coupling between the O—H groups of water. A remaining question is whether the line shape broadening of the O—H stretch spectra arises from the intermolecular vibrational coupling or intramolecular vibrational coupling. After establishing the agreement between the simulation and experiment, we quantified the strength of the intramolecular and intermolecular vibrational coupling by simulating the H_2O spectra without intermolecular coupling [20]. The data are shown in Fig. 5(a). Apparently, the line shape broadening is governed not by the intramolecular coupling but by the intermolecular coupling of the O—H stretch modes [20], consistent with the situation in bulk water [11]. Thus, the comparable vibrational coupling of bulk and interfacial water is attributable to the fact that the intermolecular vibrational coupling occurs between the interfacial water molecules in the SFG active layer with its ~5 Å thickness. The hydrogen-bonded water molecules nearest to the interface, where the effective water density is somewhat reduced, are partially SFG inactive [56].

A previous two-dimensional HD-SFG study [57] indicated that the interfacial O—H groups consist of vibrationally coupled O—H groups and vibrationally uncoupled O—H groups which are the other half of the free O—H group. This Letter further shows that the spectral diffusion of the vibrationally coupled O—H group is bulklike. Our simulation analysis (see Supplemental Material IX [33] for the definition of different types of water molecules, which includes Ref. [58]) shows that the vibrationally uncoupled O—H group does not change the FWHM, while the vibrationally coupled O—H group has a bulklike vibrational coupling (see Fig. 5(b) and Supplemental Material [33].). Therefore, the observation of the FWHM in the spectral decomposition analysis is consistent with the two-dimensional HD-SFG study [57]. Overall, the vibrationally coupled O—H groups dominate the SFG signature in the low frequency side [24,57], altering the FWHM upon the isotopic dilution.

In summary, we carried out the HD-SFG measurement at the ssp polarization combination at the air-neat H_2O (D_2O) and $\mathrm{air/H:D} = 1:4$ ($\mathrm{H:D} = 3:1$) isotopically diluted water interfaces. With the Lorentz model for the Fresnel factor correction, we confirmed a significant impact of the vibrational coupling on the $\mathrm{Im}\chi^{(2)}_{yyz}$ spectra. Through decomposing the spectra, we found that the impact of the vibrational coupling is largely suppressed due to the Fresnel factor in the $\mathrm{Im}(\chi^{(2)}_{\mathrm{eff}})_{ssp}$ spectra, solving the controversial discussion on the impact of the vibrational coupling of the interfacial water. Our analysis clarified that the vibrational coupling of water is comparable for bulk and interfacial water. The presented $\mathrm{Im}\chi^{(2)}_{yyz}$ data for HOD in D_2O is the simplest and easiest target for the theoretical modeling [15], which can be done with the frequency mapping technique [59], surface-specific velocity-velocity time correlation approach [43,60], as well as the general time correlation approach [61,62].

All data required to evaluate the conclusions in the Letter are available in the main text or in [33].

We thank Fujie Tang for stimulating discussions and Masanari Okuno for providing the IR and Raman data. The authors gratefully acknowledge support from the MaxWater initiative from the Max Planck Society. We are grateful for the financial support from the MaxWater Initiative of the Max Planck Society. Funded by the European Union (ERC, n-AQUA, 101071937).

Views and opinions expressed are however those of the author(s) only and do not necessarily reflect those of the

European Union or the European Research Council Executive Agency. Neither the European Union nor the granting authority can be held responsible for them.

The authors declare no competing financial interests.

*These authors contributed equally to this work.
†Corresponding author: bonn@mpip-mainz.mpg.de
‡Corresponding author: nagata@mpip-mainz.mpg.de

[1] Y. Nagata, K. Usui, and M. Bonn, Phys. Rev. Lett. **115**, 236102 (2015).
[2] O. Carrier, N. Shahidzadeh-Bonn, R. Zargar, M. Aytouna, M. Habibi, J. Eggers, and D. Bonn, J. Fluid Mech. **798**, 774 (2016).
[3] B. Rana, D. J. Fairhurst, and K. C. Jena, J. Am. Chem. Soc. **144**, 17832 (2022).
[4] J. E. Klijn and J. B. F. N. Engberts, Nature (London) **435**, 746 (2005).
[5] R. Kusaka, S. Nihonyanagi, and T. Tahara, Nat. Chem. **13**, 306 (2021).
[6] L. Piatkowski, K. B. Eisenthal, and H. J. Bakker, Phys. Chem. Chem. Phys. **11**, 9033 (2009).
[7] S. Woutersen and H. J. Bakker, Nature (London) **402**, 507 (1999).
[8] M. L. Cowan, B. D. Bruner, N. Huse, J. R. Dwyer, B. Chugh, E. T. J. Nibbering, T. Elsaesser, and R. J. D. Miller, Nature (London) **434**, 199 (2005).
[9] K. Ramasesha, L. De Marco, A. Mandal, and A. Tokmakoff, Nat. Chem. **5**, 935 (2013).
[10] F. Perakis, L. De Marco, A. Shalit, F. Tang, Z. R. Kann, T. D. Kühne, R. Torre, M. Bonn, and Y. Nagata, Chem. Rev. **116**, 7590 (2016).
[11] B. M. Auer and J. L. Skinner, J. Chem. Phys. **128**, 224511 (2008).
[12] W. B. Carpenter, J. A. Fournier, R. Biswas, G. A. Voth, and A. Tokmakoff, J. Chem. Phys. **147**, 084503 (2017).
[13] K. Inoue, Y. Litman, D. M. Wilkins, Y. Nagata, and M. Okuno, J. Phys. Chem. Lett. **14**, 3063 (2023).
[14] S. Nihonyanagi, T. Ishiyama, T. K. Lee, S. Yamaguchi, M. Bonn, A. Morita, and T. Tahara, J. Am. Chem. Soc. **133**, 16875 (2011).
[15] C. S. Tian and Y. R. Shen, J. Am. Chem. Soc. **131**, 2790 (2009).
[16] X. Xu, Y. R. Shen, and C. Tian, J. Chem. Phys. **150**, 144701 (2019).
[17] K. Inoue, M. Ahmed, S. Nihonyanagi, and T. Tahara, Nat. Commun. **11**, 5344 (2020).
[18] S. Nihonyanagi, R. Kusaka, K. I. Inoue, A. Adhikari, S. Yamaguchi, and T. Tahara, J. Chem. Phys. **143**, 124707 (2015).
[19] F. Tang, T. Ohto, S. Sun, J. Rouxel, S. Imoto, E. H. G. Backus, S. Mukamel, M. Bonn, and Y. Nagata, Chem. Rev. **120**, 3633 (2020).
[20] C. S. Hsieh, R. Kramer Campen, M. Okuno, E. H. G. Backus, Y. Nagata, and M. Bonn, Proc. Natl. Acad. Sci. U.S.A. **110**, 18780 (2013).
[21] J. Schaefer, E. H. G. Backus, Y. Nagata, and M. Bonn, J. Phys. Chem. Lett. **7**, 4591 (2016).
[22] S. Yamaguchi, T. Takayama, Y. Goto, T. Otosu, and T. Yagasaki, J. Phys. Chem. Lett. **13**, 9649 (2022).
[23] M. Sovago, R. K. Campen, G. W. H. Wurpel, M. Müller, H. J. Bakker, and M. Bonn, Phys. Rev. Lett. **100**, 173901 (2008).
[24] I. V. Stiopkin, C. Weeraman, P. A. Pieniazek, F. Y. Shalhout, J. L. Skinner, and A. V. Benderskii, Nature (London) **474**, 192 (2011).
[25] Y. Nagata, R. E. Pool, E. H. G. Backus, and M. Bonn, Phys. Rev. Lett. **109**, 226101 (2012).
[26] W. J. Smit, J. Versluis, E. H. G. Backus, M. Bonn, and H. J. Bakker, J. Phys. Chem. Lett. **9**, 1290 (2018).
[27] E. A. Raymond, T. L. Tarbuck, and G. L. Richmond, J. Phys. Chem. B **106**, 2817 (2002).
[28] Y. Ni and J. L. Skinner, J. Chem. Phys. **145**, 031103 (2016).
[29] B. M. Auer and J. L. Skinner, J. Phys. Chem. B **113**, 4125 (2009).
[30] X. Yu, K.-Y. Chiang, C.-C. Yu, M. Bonn, and Y. Nagata, J. Chem. Phys. **158**, 044701 (2023).
[31] J.-J. J. Max and C. Chapados, J. Chem. Phys. **131**, 184505 (2009).
[32] K.-Y. Chiang, T. Seki, C.-C. Yu, T. Ohto, J. Hunger, M. Bonn, and Y. Nagata, Proc. Natl. Acad. Sci. U.S.A. **119**, e2204156119 (2022).
[33] See Supplemental Material at http://link.aps.org/supplemental/10.1103/PhysRevLett.131.256202 for experimental details, IR and Raman spectra, simulation protocols, the dielectric spectra for $H:D = 1:4$ isotopically diluted water, detailed data processing, the phase accuracy of HD-SFG measurements, Fresnel factor spectra L_{yyz}, and the discussion of negligible contribution of uncoupled O─H group to the vibrational coupling.
[34] M. Wolfsberg, A. A. Massa, and J. W. Pyper, J. Chem. Phys. **53**, 3138 (1970).
[35] J. C. Duplan, L. Mahi, and J. L. Brunet, Chem. Phys. Lett. **413**, 400 (2005).
[36] J.-J. Max and C. Chapados, J. Chem. Phys. **116**, 4626 (2002).
[37] G. M. Hale and M. R. Querry, Appl. Opt. **12**, 555 (1973).
[38] S. Sun, R. Liang, X. Xu, H. Zhu, Y. R. Shen, and C. Tian, J. Chem. Phys. **144**, 244711 (2016).
[39] S. Yamaguchi, J. Chem. Phys. **145**, 167101 (2016).
[40] M. Ahmed, Y. Nojima, S. Nihonyanagi, S. Yamaguchi, and T. Tahara, J. Chem. Phys. **152**, 237101 (2020).
[41] T. Ishiyama and A. Morita, J. Phys. Chem. Lett. **10**, 5070 (2019).
[42] G. R. Medders and F. Paesani, J. Am. Chem. Soc. **138**, 3912 (2016).
[43] T. Ohto, K. Usui, T. Hasegawa, M. Bonn, and Y. Nagata, J. Chem. Phys. **143**, 124702 (2015).
[44] M. Ahmed, S. Nihonyanagi, and T. Tahara, J. Chem. Phys. **156**, 224701 (2022).
[45] S. Yamaguchi and T. Tahara, J. Phys. Chem. C **119**, 14815 (2015).
[46] S. Yamaguchi, K. Shiratori, A. Morita, and T. Tahara, J. Chem. Phys. **134**, 184705 (2011).
[47] M. Okuno, J. Raman Spectrosc. **52**, 849 (2021).
[48] C.-C. Yu *et al.*, Nat. Commun. **11**, 5977 (2020).

[49] P. E. Ohno, H. Wang, and F. M. Geiger, Nat. Commun. **8**, 1032 (2017).
[50] F. Wei, S. Urashima, S. Nihonyanagi, and T. Tahara, J. Am. Chem. Soc. **145**, 8833 (2023).
[51] Y.-C. Wen, S. Zha, X. Liu, S. Yang, P. Guo, G. Shi, H. Fang, Y. R. Shen, and C. Tian, Phys. Rev. Lett. **116**, 016101 (2016).
[52] S. H. Urashima, A. Myalitsin, S. Nihonyanagi, and T. Tahara, J. Phys. Chem. Lett. **9**, 4109 (2018).
[53] S. Pezzotti, D. R. Galimberti, and M.-P. Gaigeot, J. Phys. Chem. Lett. **8**, 3133 (2017).
[54] T. Ishiyama and A. Morita, J. Chem. Phys. **131**, 244714 (2009).
[55] T. Hasegawa and Y. Tanimura, J. Phys. Chem. B **115**, 5545 (2011).
[56] N. K. Kaliannan, A. Henao Aristizabal, H. Wiebeler, F. Zysk, T. Ohto, Y. Nagata, and T. D. Kühne, Mol. Phys. **118**, 1620358 (2020).
[57] C.-S. Hsieh, M. Okuno, J. Hunger, E. H. G. Backus, Y. Nagata, and M. Bonn, Angew. Chem. Int. Ed. **53**, 8146 (2014).
[58] F. Tang, T. Ohto, T. Hasegawa, W. J. Xie, L. Xu, M. Bonn, and Y. Nagata, J. Chem. Theory Comput. **14**, 357 (2018).
[59] B. M. Auer and J. L. Skinner, J. Chem. Phys. 129, **129**, 214705 (2008).
[60] R. Khatib and M. Sulpizi, J. Phys. Chem. Lett. **8**, 1310 (2017).
[61] A. Morita and J. T. Hynes, J. Phys. Chem. B **106**, 673 (2002).
[62] C. Liang, J. Jeon, and M. Cho, J. Phys. Chem. Lett. **10**, 1153 (2019).